Thrombospondin-1 triggers calreticulin expression in human mucoepidermoid carcinoma MC-3 cells via the PERK/CHOP pathway

SHENGWEI BAO[1,2*], YUANYUAN ZHU[2*], LIJUAN GUO[1,3] and SEN YANG[1,2]

[1]School of Stomatology, Zunyi Medical University, Zunyi, Guizhou 563000, P.R. China;
[2]Department of Oral and Maxillofacial Surgery, Suining Central Hospital, Suining, Sichuan 629000, P.R. China;
[3]Department of Aesthetic Medicine, Suining Central Hospital, Suining, Sichuan 629000, P.R. China

Received August 15, 2025; Accepted March 20, 2026

DOI: 10.3892/ol.2026.15589

Abstract. Mucoepidermoid carcinoma (MEC) is the most common salivary gland malignancy, accounting for ~30% of all salivary gland malignancies; however, effective treatments for advanced-stage disease remain limited. The induction of immunogenic cell death (ICD) has emerged as a potent anti-tumor intervention for MEC. Thrombospondin-1 (TSP-1) exhibits documented anti-tumor properties in MEC; however, its capacity to drive ICD-mediated tumor suppression remains poorly understood. In the present study, the mechanistic role of TSP-1 was investigated in MC-3 cells across four experimental cohorts: Control, TSP-1, TSP-1 combined with a PERK inhibitor (ISRIB) and TSP-1 combined with a PERK activator (CCT020312). Cellular assays, including flow cytometry, immunofluorescence and western blot analysis, revealed that TSP-1 triggered ICD at 72 h, characterized by a significant increase in calreticulin (CRT) surface exposure. Mechanistically, pharmacological inhibition of PERK attenuated the expression of the PERK/CHOP axis. Notably, while the 4 h TSP-1 monotherapy showed negligible effects on CRT, the integration of the PERK inhibitor markedly diminished PERK/CHOP/CRT signaling. Collectively, the present data indicated that TSP-1 facilitated ICD and CRT translocation in MEC cells via the activation of the PERK/CHOP signaling cascade. These results provide a rationale for further *in vivo* investigations to substantiate the therapeutic potential of TSP-1-induced ICD in MEC management.

Correspondence to: Professor Sen Yang, Department of Oral and Maxillofacial Surgery, Suining Central Hospital, 127 Desheng West Road, Suining, Sichuan 629000, P.R. China
E-mail: ys13880435413@163.com

Professor Lijuan Guo, Department of Aesthetic Medicine, Suining Central Hospital, 127 Desheng West Road, Suining, Sichuan 629000, P.R. China
E-mail: 663418587@qq.com

*Contributed equally

Abbreviations: MEC, mucoepidermoid carcinoma; ICD, immunogenic cell death; TSP-1, thrombospondin-1; CRT, calreticulin

Key words: immunogenic cell death, thrombospondin-1, MC-3 cells, calreticulin, PERK/CHOP signaling pathway

Introduction

Mucoepidermoid carcinoma (MEC) is the most prevalent malignancy of the salivary glands, accounting for ~30% of all salivary gland malignancies and 10-15% of all salivary gland tumors (1,2). Tumor staging and grading serve as notable prognostic indicators for patient survival. Notably, the rate of cervical lymph node metastasis in MEC reaches as high as 36.9% globally, surpassing the regional lymph node metastasis rate of 27.2% (3,4). Although surgery remains the primary treatment modality for malignant MEC, neither surgery alone nor chemotherapy alone yields favorable survival outcomes, leading to a relatively low overall survival rate (5). For patients with advanced-stage disease, distant metastasis or those who are ineligible for surgery, effective therapeutic options are currently lacking. Compared with conventional approaches, the research and application of immunotherapy in various cancer types have markedly enhanced treatment efficacy (6,7). Therapeutic strategies that induce tumor cell death, elicit specific anti-tumor immune responses and establish long-lasting immune memory are widely regarded as superior choices for anti-tumor therapy (8-10).

As a central form of programmed cell death, the initiation and execution of apoptosis are finely regulated by various signals within the tumor microenvironment (TME). Extensive research has demonstrated that cytokines and inflammatory mediators secreted by immune effector cells can actively induce apoptosis in target cells. This process is characterized by a series of morphological and molecular alterations, such as the loss of mitochondrial membrane potential, activation of the caspase cascade and DNA fragmentation. These changes constitute the hallmarks of induced apoptosis and provide the molecular foundation for immune-mediated cell death (11). Within the TME, cytokines such as tumor necrosis factor-α, released by immune

effectors, bind to death receptors such as CD95/Fas on the target cell surface, directly activating extrinsic apoptotic pathways and determining the fate of tumor cells (12). Such apoptosis triggered by immune mediators is closely linked to immunogenic cell death (ICD). The core feature of ICD is that dying tumor cells express or release a series of damage-associated molecular patterns (DAMPs) (13-16), including calreticulin (CRT), adenosine triphosphate (ATP), annexin A1, type I interferons and high mobility group protein B1 (HMGB1). These DAMPs activate the host immune system and promote the establishment of anti-tumor immune responses (17,18). Notably, CRT is a soluble protein localized in the endoplasmic reticulum (ER) that translocates from the ER to the cell surface via the Golgi apparatus under ER stress. This translocation is typically mediated by protein kinase RNA-like ER kinase (PERK)-induced phosphorylation of eukaryotic initiation factor 2α (eIF2α). Subsequently, caspase-8-mediated BAP31 activation triggers pro-apoptotic proteins such as BAX and BAK, leading to apoptosis. Furthermore, C/EBP homologous protein (CHOP) serves as a notable pro-apoptotic transcription factor during ER stress-induced apoptosis, and the PERK/CHOP signaling pathway is recognized as a classical axis in ER stress-related apoptotic research (19-22).

Various clinical drugs and treatment modalities have been confirmed to induce ICD. Chemotherapeutic agents include doxorubicin (DOX), oxaliplatin (OXA), cyclophosphamide and paclitaxel (PTX) (23), while other modalities encompass photodynamic therapy, photothermal therapy, radiotherapy and sonodynamic therapy (24-27). In this context, developing strategies that can effectively eradicate MEC cells and induce ICD to elicit a systemic anti-tumor immune response represents a research direction.

Thrombospondin-1 (TSP-1) is a multifunctional protein that influences multiple aspects of tumor progression, including angiogenesis, tumor growth, cell morphology, adhesion and migration, serving as a key player in the TME (28). Miao *et al* (29) found that TSP-1 can inhibit the growth of melanoma through its type 1 repeats, which exert anti-angiogenic effects via both TGF-β-dependent and-independent mechanisms. Additionally, Uscanga-Palomeque *et al* (30) developed the CD47 agonist peptide PKHB1 based on the C-terminus of TSP-1 and discovered its ability to induce ICD in T-cell acute lymphoblastic leukemia. However, while most research on TSP-1 has focused on its anti-angiogenic and growth-inhibitory properties, to the best of our knowledge, reports regarding its role in inducing ICD are limited. Therefore, the present study focuses on TSP-1 to explore its potential in inhibiting growth and triggering ICD in MEC.

In our previous research, it was demonstrated that TSP-1 inhibits the growth and migration of MEC cell lines and promotes apoptosis, and subsequent investigations revealed that TSP-1 increases the release of DAMPs and induces ICD in the MC-3 cell line (31). Given the therapeutic advantages of TSP-1 in MC-3 cells, the present study further investigated the molecular mechanism underlying TSP-1-induced CRT translocation. Specifically, whether this process is mediated by the PERK/CHOP signaling pathway. The present research aimed to elucidate the mechanistic role of TSP-1 in MC-3 cells, thereby providing an experimental foundation for its future therapeutic application in MEC.

Materials and methods

Cell culture. The MC-3 cell line was provided by the Department of Biology, School of Stomatology, Air Force Medical University, Xi'an, China (serial no. AFMU-BIO-003). The cells were maintained in DMEM supplemented with 10% fetal bovine serum (both from Gibco; Thermo Fisher Scientific, Inc.) and cultured in a humidified incubator at 37˚C with 5% CO_2.

Flow cytometric detection of surface-presented CRT. MC-3 cells were seeded into 6-well plates and cultured overnight to allow for adherence. The cells were subsequently assigned to five experimental groups: Isotype control, blank control, TSP-1, TSP-1 + ISRIB (a PERK inhibitor) and TSP-1 + CCT020312 (a PERK activator). TSP-1 (Novoprotein Scientific Inc.) was used at a concentration of 0.1 μmol/l, ISRIB (cat. no. 548470-11-7; Medchemexpress) was used at 10 nmol/l and CCT020312 (cat. no. 324759-76-4; Medchemexpress) was used at 20 μmol/l. Following treatment for either 4 or 72 h at 37˚C, cells were harvested and washed twice with ice-cold PBS. For surface staining, the cells were incubated with a primary anti-CRT antibody (1:100; cat. no. ET1068-60; HUABIO) or an isotype-matched control antibody (1:100; cat. no. ab172730; Abcam) for 1 h at room temperature in the dark. After washing, the cells were incubated with a fluorescent secondary antibody (iFluor 647; 1:500; cat. no. HA1123; HUABIO) under the same conditions for an additional 1 h. Finally, the cells were resuspended in 0.3 ml of PBS and analyzed using the APC channel of a flow cytometer (CytoFLEX S; Beckman Coulter).

Immunofluorescence. After treatment for the specified durations (4 and 72 h), MC-3 cells cultured on coverslips were pre-washed with PBS and fixed with 4% paraformaldehyde at room temperature for 20 min. Following the wash steps, all samples except those designated for CRT detection were permeabilized with 0.5% Triton X-100 for 30 min at room temperature. After blocking with goat serum (cat. no. BL1092A; Biosharp Life Sciences) for 30 min, the cells were incubated with primary antibodies (anti-PERK; cat. no. HA721510; anti-CHOP; cat. no. HA722854; anti-CRT; cat. no. ET1068-60; HUABIO) at a dilution of 1:200 at room temperature for 2 h in a humidified incubator. Subsequently, the cells were incubated with fluorescently labeled secondary antibodies (iFluor 594; 1:200; cat. no. HA1122; HUABIO) for 1 h at room temperature in the dark, followed by nuclear staining with DAPI at room temperature for 5 min. After mounting, images were captured using a fluorescence microscope (EVOS M5000; Thermo Fisher Scientific, Inc.) at x400 magnification.

Reverse transcription-quantitative (RT-q)PCR. Total RNA was extracted from cells using the TRIzol universal method (32) (DP424; Tiangen Biotech Co., Ltd.). For cDNA synthesis, 1 μg of total RNA was reverse-transcribed using a reverse transcription kit (Thermo Fisher Scientific, Inc.). The reverse transcription reaction was performed at 42˚C for 15 min, followed by inactivation at 95˚C for 5 min. qPCR was subsequently conducted using SYBR Green PCR Master Mix (TaKaRa Biotechnology Co., Ltd.) on a CFX96 Real-Time PCR Detection System (Bio-Rad, USA). The thermal cycling

conditions were as follows: Initial denaturation at 95˚C for 3 min; 40 cycles of denaturation at 95˚C for 15 sec, annealing at 60˚C for 30 sec, and extension at 72˚C for 30 sec; followed by melting curve analysis from 65˚C to 95˚C with increments of 0.5˚C per 5 sec to confirm product specificity. The relative expression levels of target genes were calculated using the $2^{-\Delta\Delta Cq}$ method (33), with GAPDH serving as the endogenous reference gene. Currently, various molecular biology techniques are widely employed to investigate genetic alterations (34); in the present study, the RT-qPCR method was selected to ensure high sensitivity and accuracy. All primers were synthesized by Beijing Tsingke Biotech Co., Ltd.. The primer sequences were as follows: PERK, forward 5'-AGCCAATTCAATGCCTGGGA-3' and reverse 5'-ACTTCTCTGGTGGTGCTTCG-3'; CHOP, forward 5'-TTAAAGATGAGCGGGTGGCA-3' and reverse 5'-ACTTTCTTGAACACTCTCTCC-3'; CRT, forward 5'-AGCAGAACATCGACTGTGGG-3' and reverse 5'-CCACAGATGTCGGGACCAAA-3'; GAPDH forward 5'-GGAGTCCACTGGCGTCTTCA-3' and reverse 5'-GTCATGAGTCCTTCCACGATACC-3'.

Western blotting (WB). Total protein was extracted from MC-3 cells in each group using RIPA lysis buffer (cat. no. AR0102S; (Wuhan Boster Biological Technology, Ltd.). After determining protein concentrations via the BCA assay, 25 μg of protein per lane were separated by 12% SDS-PAGE (Beijing Solarbio Science & Technology Co., Ltd.) and subsequently transferred onto PVDF membranes (MilliporeSigma), following the protocol described by Jurisic *et al* (35). The membranes were blocked in TBS-Tween (TBST; 0.1% Tween 20) containing 5% BSA (cat. no. ST023-50g; Beyotime Biotechnology) for 1 h at room temperature. Primary antibodies, including anti-PERK (1:1,000; cat. no. MA8131; Abmart Pharmaceutical Technology Co., Ltd.), anti-CHOP (1:1,000; cat. no. WL00880; Wanleibio Co., Ltd.), anti-CRT (1:800; cat. no. bs-5913R; BIOSS) and anti-β-actin (1:5,000; cat. no. 66009-1-Ig; Proteintech Group Inc.), were diluted in 5% BSA and incubated with the membranes overnight at 4˚C. After washing with TBST, the membranes were incubated with secondary antibodies (1:5,000; cat. nos. SA00001-1 and SA00001-2; Proteintech Group Inc.) for 1 h at room temperature. Following three additional washes with TBST, protein bands were visualized using an ECL chemiluminescence detection kit (cat. no. BMU102; Abbkine Scientific Co., Ltd.) in the dark and captured using an imaging system.

Statistical methods. Statistical analysis was performed using GraphPad Prism 10.0 software (Dotmatics). Data are presented as the mean ± standard deviation. Comparisons between two groups were conducted using the independent-samples t-test, whereas multiple group comparisons were analyzed using one-way analysis of variance (ANOVA) followed by Tukey's post hoc test. $P<0.05$ was considered to indicate a statistically significant difference. All experiments were repeated three times.

Results

TSP-1 upregulates cell surface CRT expression in MC-3 cells. To investigate the mechanism by which TSP-1 induces ICD in MC-3 cells, the surface expression of CRT was first evaluated. Flow cytometry analysis revealed that following 72 h of TSP-1 treatment, the mean fluorescence intensity of CRT on the MC-3 cell membrane was significantly increased ($P<0.01$) (Fig. 1). To further elucidate the underlying mechanism, the regulatory role of ER stress and its downstream PERK/CHOP signaling pathway in CRT translocation was investigated. By employing the PERK inhibitor ISRIB and the activator CCT020312, it was discovered that ISRIB partially reversed the TSP-1-induced CRT expression ($P<0.05$), whereas CCT020312 further synergistically enhanced this effect ($P<0.05$). These results suggest that the PERK pathway is involved in the process of TSP-1-induced surface translocation of CRT.

TSP-1 induces protein localization of PERK, CHOP and CRT at 72 h. After treating MC-3 cells with TSP-1 in combination with ISRIB or CCT020312 for 72 h, the expression levels of PERK, CHOP and CRT were evaluated via immunofluorescence. The fluorescence intensities reflected the cytoplasmic levels of PERK and CHOP, as well as the surface expression of CRT, with higher intensity indicating increased protein abundance. In the TSP-1-treated group, PERK expression was significantly elevated compared with the control group ($P<0.01$). The TSP-1 + ISRIB group exhibited significantly reduced PERK expression compared with the TSP-1 group ($P<0.05$). Notably, the combination of TSP-1 and CCT020312 yielded the highest PERK fluorescence intensity ($P<0.01$) (Fig. 2). The expression patterns of CHOP and CRT across all groups were consistent with those of PERK (Figs. 3 and 4). These findings demonstrated that TSP-1 upregulated PERK/CHOP pathway components and CRT expression, a process that is positively regulated by PERK activity.

TSP-1 upregulates ER stress-related genes. To clarify the impact of TSP-1 on the ER stress pathway at the transcriptional level, RT-qPCR was performed to evaluate the mRNA expression of PERK, CHOP and CRT in MC-3 cells after 72 h of treatment. The results showed that the mRNA levels of all three targets were significantly upregulated ($P<0.05$) with TSP-1 treatment compared with control, consistent with the previously observed protein fluorescence patterns (Fig. 5). Furthermore, analysis revealed that inhibiting PERK resulted in a significant reduction in CHOP expression ($P<0.05$; Fig. 5B), whereas activating PERK led to a synchronized increase in both CHOP and CRT expression (Fig. 5B and C; $P<0.05$). These findings suggest that TSP-1 mediates CRT expression in MC-3 cells via the PERK/CHOP signaling pathway.

Protein expression of CHOP and CRT after 72 h treatment. WB analysis further confirmed these findings at the protein level (Fig. 6). Compared with the control group, TSP-1 treatment for 72 h significantly increased the protein expression levels of CHOP and CRT ($P<0.01$). Conversely, co-treatment with ISRIB reduced the expression of these two proteins ($P<0.05$), whereas co-treatment with CCT020312 further elevated their expression ($P<0.05$). These results are consistent with the activation of ER stress and its downstream signaling pathways, which are core features of ICD. Studies have indicated that the PERK/CHOP pathway is a critical signaling axis for ER stress-induced apoptosis and ICD, with persistent

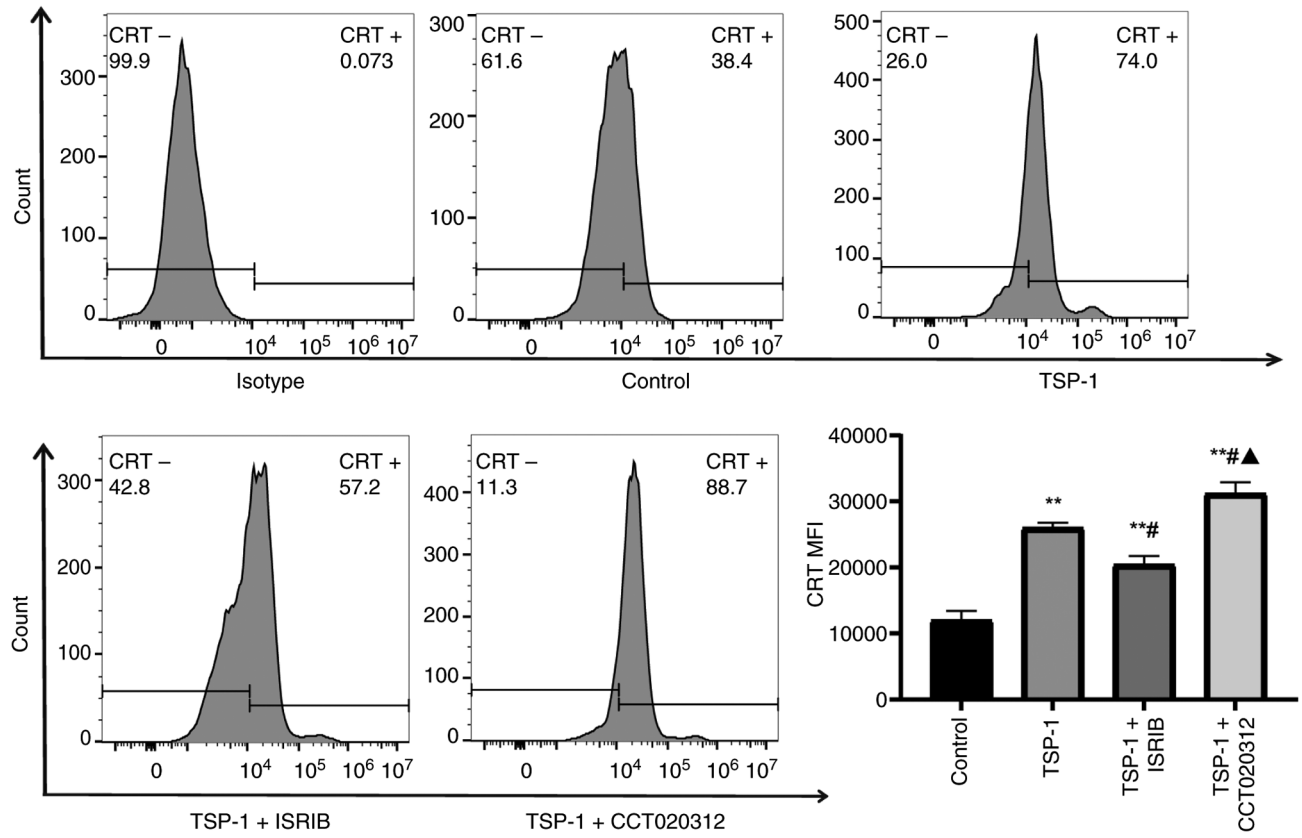

Figure 1. TSP-1 promotes the translocation of CRT to the cell surface in MC-3 cells. Cells were stained with an APC-conjugated anti-CRT antibody, and CRT expression on the cell membrane is presented as mean fluorescence intensity. At the 72 h point: **P<0.01 vs. the control group; $^{\#}$P<0.05 vs. the TSP-1 group; and $^{\blacktriangle}$P<0.05 vs. the TSP-1 + ISRIB group. MFI, mean fluorescence intensity; CRT, calreticulin; TSP-1, thrombospondin-1.

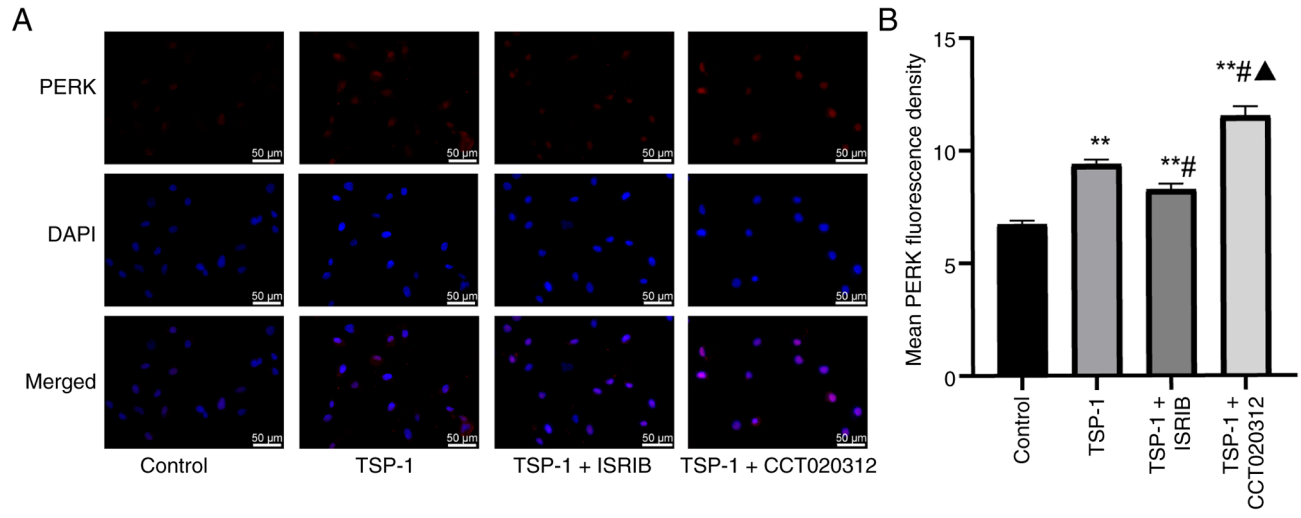

Figure 2. PERK immunofluorescence in MC-3 cells at 72 h. (A) PERK immunofluorescence in MC-3 cells at 72 h (x400; scale bar, 50 μm). (B) Immunofluorescence detection of PERK expression in each group. Red fluorescence shows cytoplasmic PERK expression, DAPI staining shows blue fluorescence in the same field of view; merge is the merged result of red fluorescence and DAPI blue fluorescence. **P<0.01 compared with control group; $^{\#}$P<0.05 compared with TSP-1 action group; and $^{\blacktriangle}$P<0.05 compared with TSP-1 + ISRIB group. TSP-1, thrombospondin-1.

high expression of CHOP serving as a major driver of terminal apoptosis (36). In the present study, TSP-1 effectively activated the PERK/CHOP pathway in MC-3 cells, leading to the upregulation of the key ICD marker CRT. This process was positively regulated by PERK kinase activity. Collectively, these results establish the molecular mechanism by which TSP-1 induces CRT expression via the PERK/CHOP pathway at the protein level.

mRNA expression of PERK, CHOP and CRT at 4 h. The mRNA expression levels of PERK, CHOP and CRT in MC-3 cells were evaluated by RT-qPCR after 4 h of treatment (Fig. 7).

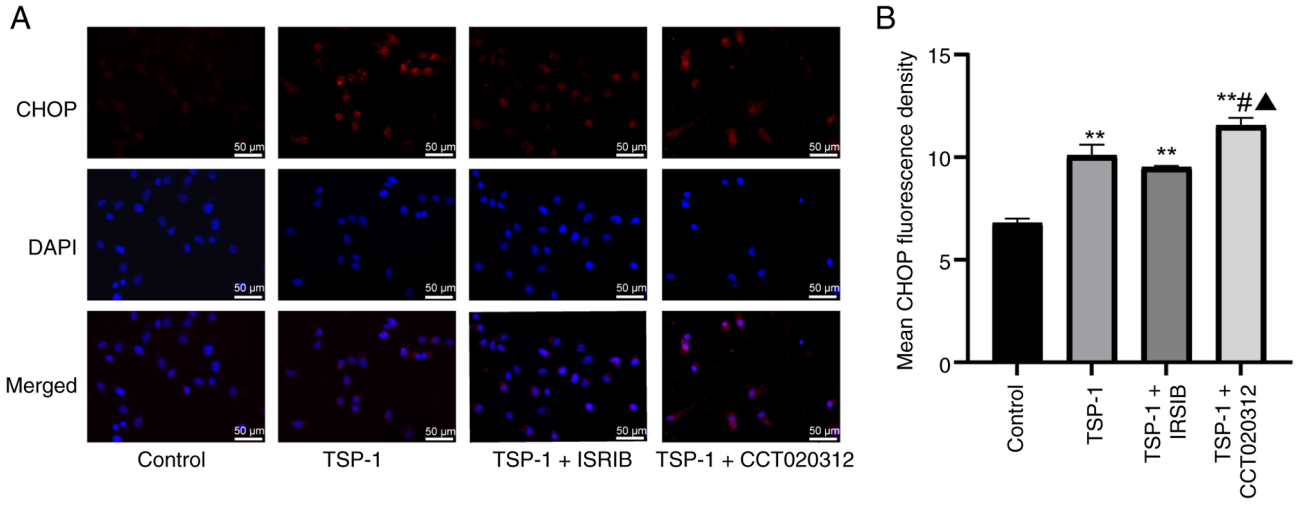

Figure 3. CHOP immunofluorescence in MC-3 cells at 72 h. (A) Immunofluorescence staining for CHOP in MC-3 cells at 72 h (x400; scale bar, 50 μm). (B) Immunofluorescence detection of CHOP expression in each group. Red fluorescence shows cytoplasmic CHOP expression, DAPI staining shows blue fluorescence in the same field of view; merge is the merged result of red fluorescence and DAPI blue fluorescence. **P<0.01 compared with control group; $^{\#}$P<0.05 compared with TSP-1 action group; and $^{\blacktriangle}$P<0.05 compared with TSP-1 + ISRIB group. TSP-1, thrombospondin-1.

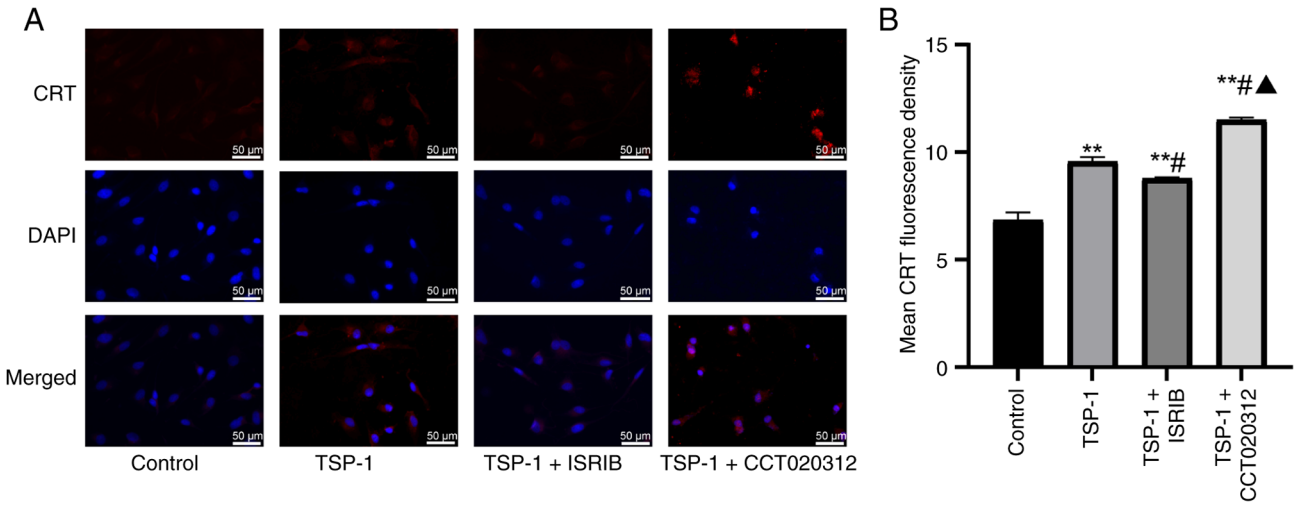

Figure 4. CRT immunofluorescence in MC-3 cells at 72 h. (A) Immunofluorescence staining of CRT in MC-3 cells at 72 h (x400; scale bar, 50 μm). (B) Immunofluorescence detection of CRT expression in each group. Red fluorescence shows cytoplasmic CRT expression, DAPI staining shows blue fluorescence in the same field of view; merge is the merged result of red fluorescence and DAPI blue fluorescence. **P<0.01 compared with control group; $^{\#}$P<0.05 compared with TSP-1 action group; and $^{\blacktriangle}$P<0.05 compared with TSP-1 + ISRIB group. TSP-1, thrombospondin-1; CRT, calreticulin.

The results demonstrated that no statistically significant differences in PERK, CHOP or CRT mRNA levels were observed between the TSP-1 group and the control group, suggesting that TSP-1 had a limited effect on MC-3 cells at the 4 h time point. Furthermore, co-treatment with ISRIB did not significantly downregulate the expression of these genes, whereas co-treatment with CCT020312 resulted in significant upregulation (P<0.05). These findings further support the conclusion that PERK pathway activity is a factor regulating downstream gene expression during the early stages of treatment.

Protein localization of PERK and CRT at 4 h. At the early 4-h time point, immunofluorescence results revealed that TSP-1 treatment alone failed to significantly alter the protein expression levels of PERK and CRT (Fig. 8). Conversely, co-treatment with the PERK inhibitor ISRIB significantly reduced the expression (P<0.05) of both proteins, whereas co-treatment with CCT020312 significantly enhanced (P<0.05) them. These findings indicate that, during the early stage, changes in CRT expression are directly modulated by the activation status of PERK, and TSP-1 alone is insufficient to fully activate this signaling pathway.

Cell surface CRT expression following TSP-1 treatment at 4 h. The results indicated that a 4-h treatment with TSP-1 was insufficient to significantly enhance the cell surface expression of CRT (Fig. 9), suggesting that its effect may require a longer duration to accumulate ER stress signals. Furthermore, co-treatment with the PERK pathway activator CCT020312 significantly induced CRT expression (P<0.01). This not only confirms that activation of the PERK pathway is sufficient to drive CRT translocation but also indicates that TSP-1 fails to

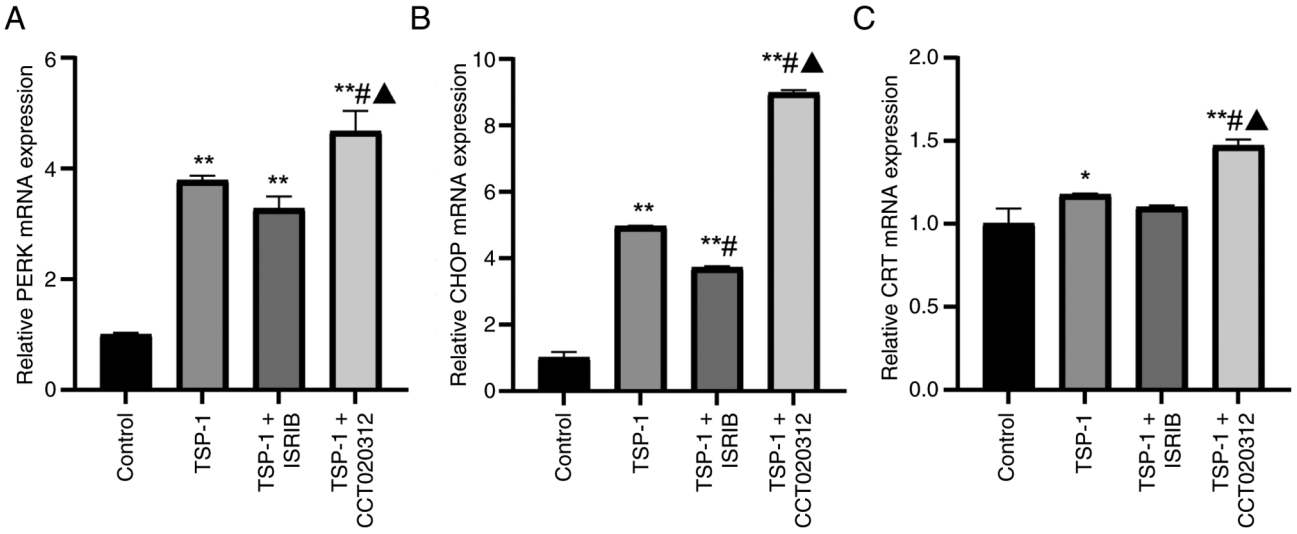

Figure 5. mRNA expression of PERK, CHOP and CRT in MC-3 cells at 72 h. (A) mRNA expression of PERK in each group at 72 h. (B) mRNA expression of CHOP in each group at 72 h. (C) mRNA expression of CRT in each group at 72 h. *P<0.05 and **P<0.01 compared with control group; #P<0.05 compared with TSP-1 action group; and ▲P<0.05 compared with TSP-1 + ISRIB group. TSP-1, thrombospondin-1; CRT, calreticulin.

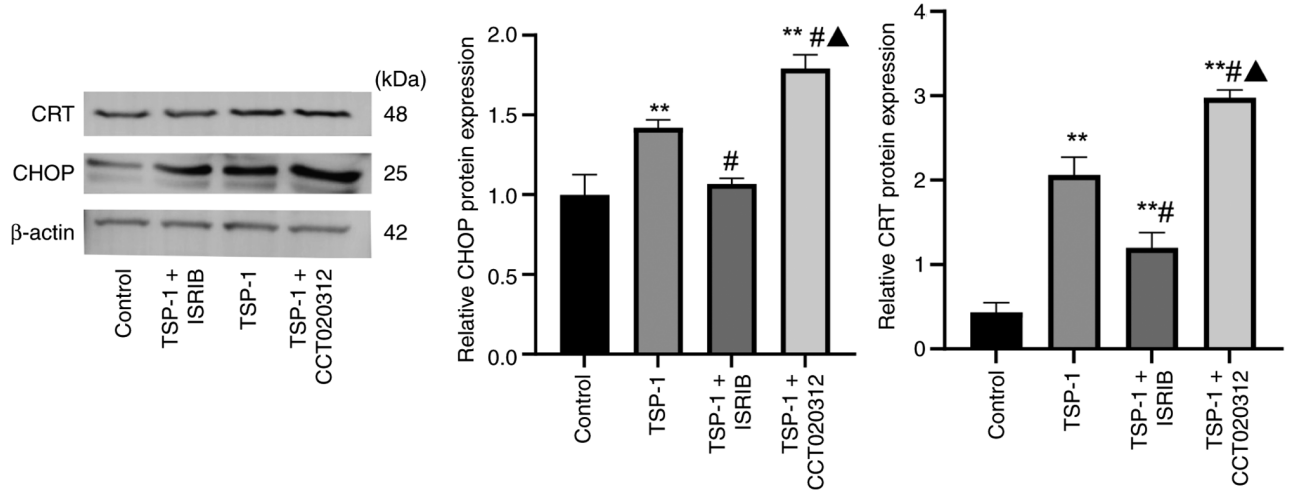

Figure 6. CHOP and CRT protein expression levels in different experimental groups. Protein expression levels of CHOP and CRT in MC-3 cells were determined by western blotting at 72 h. **P<0.01 compared with control group; #P<0.05 compared with TSP-1 action group; and ▲P<0.05 compared with TSP-1 + ISRIB group. TSP-1, thrombospondin-1; CRT, calreticulin.

effectively activate the PERK pathway at this early stage. This stands in contrast to the significant effects observed at 72 h, collectively revealing that the regulation of CRT exposure by TSP-1 via the PERK pathway was a time-dependent process.

Discussion

Based on preliminary findings (31) of the present group, the current study utilized treatment with 0.1 μmol/l TSP-1 for 72 h as the primary experimental condition to systematically explore the potential molecular mechanisms by which TSP-1 induces ICD in human MEC MC-3 cells. The present results demonstrated that TSP-1 significantly upregulated the expression of the ER stress-related molecule PERK and its downstream transcription factor CHOP, accompanied by elevated CRT expression. These findings suggest that TSP-1 may regulate the immunogenic death of MC-3 cells by activating the ER stress-PERK/CHOP signaling axis. Mechanistically, this discovery aligns TSP-1 with classical ER stress-dependent ICD inducers, such as DOX and OXA (37). However, TSP-1 may offer several advantages, including lower systemic toxicity due to its endogenous nature, the potential for targeted modulation of the tumor microenvironment and a favorable safety profile for combination therapy (28), highlighting its potential therapeutic value in the treatment of MEC.

Cell death is not a solitary event but a dynamic process characterized by distinct stages and morphological features. Research indicates that apoptosis typically progresses through early, middle and late stages, with morphological hallmarks including cell shrinkage, chromatin condensation, nuclear fragmentation, membrane blebbing and the formation of apoptotic bodies, while membrane integrity is generally maintained during the early and middle phases (38). By contrast, necrosis is characterized by rapid cell swelling, organelle rupture

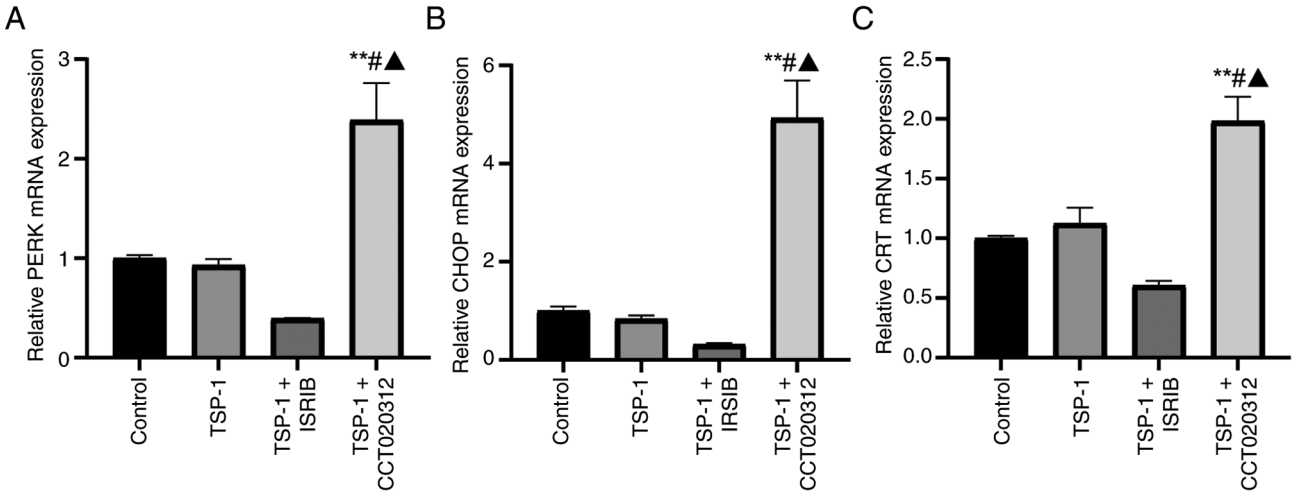

Figure 7. mRNA expression of PERK, CHOP, and CRT in MC-3 cells at 4 h. (A) mRNA expression of PERK in each group at 4 h. (B) mRNA expression of CHOP in each group at 4 h. (C) mRNA expression of CRT in each group at 4 h. **P<0.01 compared with control group; #P<0.05 compared with TSP-1 action group; and ▲P<0.05 compared with TSP-1 + ISRIB group. TSP-1, thrombospondin-1; CRT, calreticulin.

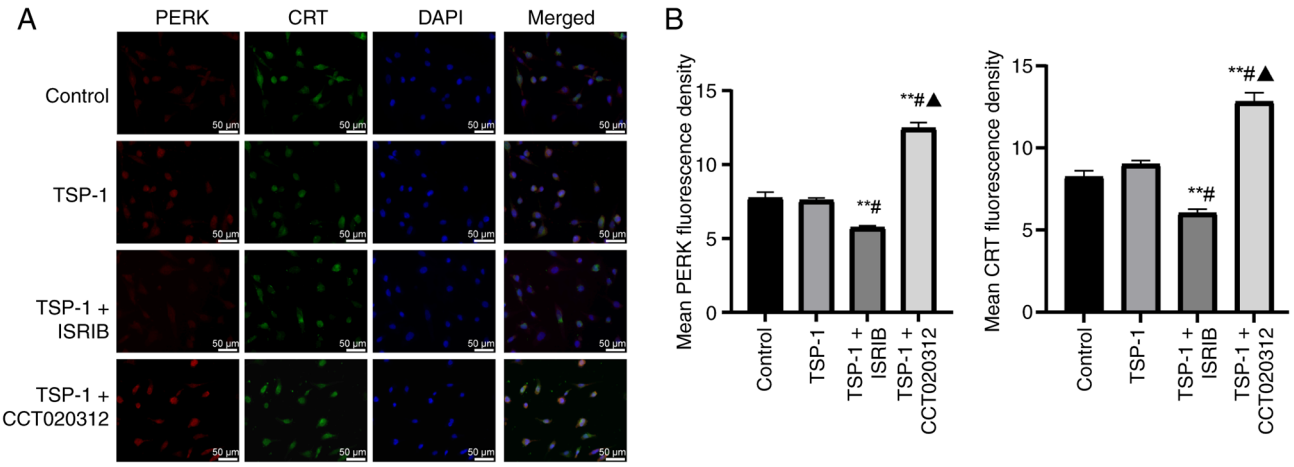

Figure 8. PERK and CRT immunofluorescence in MC-3 cells at 4 h. (A) Immunofluorescence staining of PERK and CRT in MC-3 cells (x400; scale bar, 50 μm). (B) Immunofluorescence detection of PERK and CRT in each group. PERK is indicated by red fluorescence, CRT by green fluorescence, DAPI by blue fluorescence and Merge indicates the synthesis of PERK, CRT and DAPI, respectively. **P<0.01 compared with control group; #P<0.05 compared with TSP-1 action group; and ▲P<0.05 compared with TSP-1 + ISRIB group. TSP-1, thrombospondin-1; CRT, calreticulin.

and loss of membrane integrity, leading to the uncontrolled release of intracellular contents and a potent inflammatory response (39). Notably, ICD is not simply equivalent to apoptosis or necrosis; rather, it is a specialized form of cell death that retains apoptotic morphology while simultaneously releasing immuno-stimulatory signals. The crux of ICD lies in specific subcellular and molecular events, such as ER stress, CRT translocation and the release of ATP and HMGB1, occurring in a precise temporal sequence, thereby endowing the inherently 'immuno-silent' apoptotic process with immunogenicity (40). Therefore, understanding the stages of cell death from both morphological and chronological perspectives is essential for the correct interpretation of ICD-related molecular events.

Previous studies have confirmed that the occurrence of ICD is notably dependent on ER stress and the subsequent unfolded protein response (UPR) (41,42). As one of the three primary transmembrane sensors of the UPR, the downstream PERK/eIF2α/CHOP signaling axis is considered the classical pathway mediating the translocation of CRT from the ER lumen to the cell membrane (43,44). In the present study, it was observed that TSP-1 treatment significantly upregulated PERK and CHOP expression in MC-3 cells. Furthermore, pharmacological intervention in PERK signaling correspondingly modulated the overall expression of CRT; the PERK inhibitor ISRIB attenuated the TSP-1-induced upregulation of CHOP and CRT, whereas the PERK activator CCT020312 further amplified these effects. These results were consistent at both the transcriptional and protein levels, supporting the pivotal role of the PERK/CHOP pathway in the regulation of TSP-1-induced ER stress markers.

Existing literature suggests that CRT dynamics exhibit a distinct time-dependency. For instance, classical Type I ICD inducers such as DOX and mitoxantrone can trigger CRT membrane translocation within 2-4 h of treatment, whereas Type II ICD inducers, such as photodynamic therapy, can induce CRT-related changes as early as 1 h

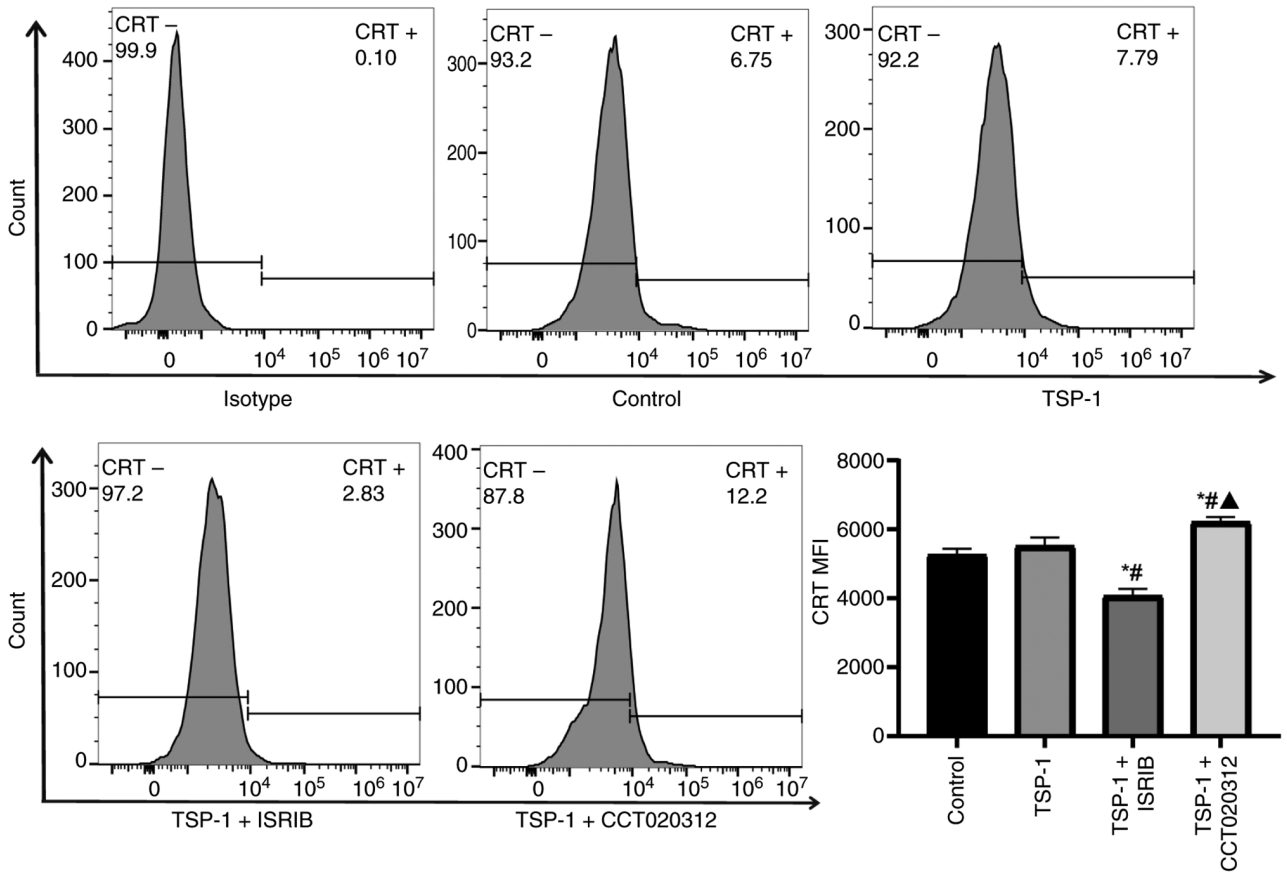

Figure 9. TSP-1 effects on cell surface CRT expression at 4 h. Cells were stained with an APC-conjugated anti-CRT antibody, and CRT expression on the cell membrane is presented as mean fluorescence intensity. At the 4 h time point. *P<0.05 compared with control group; #P<0.05 compared with TSP-1 action group; and ▲P<0.05 compared with TSP-1 + ISRIB group. TSP-1, thrombospondin-1; CRT, calreticulin.

after treatment (45-47). Based on these precedents, 4 h was selected as an early time point to observe the initial molecular events of TSP-1-induced ICD. However, at this interval, TSP-1 had not yet elicited significant activation of the PERK/CHOP pathway or detectable changes in CRT expression. Notably, even at this early stage, pharmacological modulation of PERK signaling influenced CRT expression levels, as evidenced by the finding that the PERK activator CCT020312 significantly upregulated CRT expression while the PERK inhibitor ISRIB significantly downregulated it at 4 h, suggesting that CRT regulation may be linked to PERK activity early on, though it had not yet reached the threshold required to trigger significant molecular shifts. These findings suggest that the molecular process of TSP-1-induced ICD may possess 'delayed-onset' or 'progressive accumulation' kinetic characteristics, distinguishing its mode of action from that of classical small-molecule chemotherapeutics. Furthermore, the possibility of PERK/CHOP-independent parallel or alternative pathways, such as the IRE1α-XBP1 branch of the unfolded protein response or the caspase-8/BAP31 pathway (19,22), participating in initial CRT regulation cannot be excluded. Future studies should incorporate finer time gradients and multi-pathway intervention strategies to systematically elucidate the early molecular networks and temporal features of TSP-1-induced ICD.

It is worth emphasizing that the role of the PERK pathway in ICD may extend beyond CRT-related events. PERK-mediated eIF2α phosphorylation globally regulates protein synthesis and selectively induces transcription factors such as ATF4, thereby coordinating the expression of various genes involved in stress, apoptosis and immune modulation (48). Combined with our previous finding that TSP-1 promotes the release of other DAMPs, such as ATP and HMGB1 (31), the PERK/CHOP pathway may serve as a 'hub' for coordinating the formation of the complete immunogenic death phenotype.

From a clinical translation perspective, the present results provide a theoretical foundation for the potential application of TSP-1. First, the combination of TSP-1 with chemotherapeutic agents such as PTX may enhance cytotoxicity while simultaneously bolstering the ICD effect, potentially overcoming chemoresistance in some cases of MEC. Furthermore, the DAMPs released during TSP-1-induced ICD can promote dendritic cell maturation and antigen presentation (31,49), offering a strategy to remodel the tumor microenvironment from an immunologically 'cold' state with low T cell infiltration to a 'hot' state with abundant activated T cells, and providing a rationale for combination with immune checkpoint inhibitors. Finally, the dual biological functions of TSP-1, encompassing both anti-angiogenic potential via CD36 and immunomodulatory capacity (50) may offer unique therapeutic advantages in MEC, which is typically characterized by a rich blood supply.

Despite these insights, the present study has limitations. First, the present conclusions are primarily based on *in vitro* cell models; whether TSP-1 can induce a functional anti-tumor

immune response *in vivo* requires validation in animal models. Second, while PERK/CHOP axis was the primary focus, the contributions of other UPR branches such as IRE1α-XBP1 and ATF6 (51) have not been systematically evaluated. Furthermore, although immunofluorescence and flow cytometry confirmed surface CRT expression, the temporal kinetics of translocation and its impact on the strength and duration of the *in vivo* immune response remain unclear. Finally, while pharmacological agents demonstrated the involvement of the PERK/CHOP pathway, a causal relationship has yet to be further verified using genetic approaches.

Moving forward, future studies plan to construct a humanized immune system MEC mouse model to systematically evaluate the *in vivo* efficacy of TSP-1-induced ICD and the resulting anti-tumor immune response. *In vivo* models will also be combined with multi-pathway intervention strategies to resolve the comprehensive molecular network of TSP-1-induced ICD and assess its potential for combination therapy.

Acknowledgements

Not applicable.

Funding

The present study received funding from the Provincial Science and Technology Plan Project of Sichuan Provincial Department of Science and Technology (grant no. 2022SNZY001), Sichuan Provincial Health Commission Science and Technology Project (Suitable Technology Base) (grant no. 2022JDXM021), Clinical Research Fund for Western Stomatology of the Chinese Stomatological Association (grant no. CSA-W2023-0 3) and the General Program of Sichuan Provincial Administration of Traditional Chinese Medicine (grant no. 2024MS643).

Availability of data and materials

The data generated in the present study may be requested from the corresponding author.

Authors' contributions

SY, SB and YZ designed the study and performed the experiments. SY, SB, YZ and LG performed data analysis. SB and SY drafted the manuscript and revised the manuscript. All authors read and approved the final manuscript. SY and LG confirm the authenticity of all the raw data.

Ethics approval and consent to participate

Not applicable.

Patient consent for publication

Not applicable.

Competing interests

The authors declare that they have no competing interests.

References

1. Costa RF, de Oliveira CA, Gomes ÁNM, Lourenço SV and Coutinho-Camillo CM: Molecular aspects of mucoepidermoid carcinoma and adenoid cystic carcinoma of the salivary gland. Head Neck Pathol 18: 34, 2024.
2. Sama S, Komiya T and Guddati AK: Advances in the treatment of mucoepidermoid carcinoma. World J Oncol 13: 1-7, 2022.
3. Peraza A, Gómez R, Beltran J and Amarista FJ: Mucoepidermoid carcinoma. An update and review of the literature. J Stomatol Oral Maxillofac Surg 121: 713-720, 2020.
4. Wang X, Bai J, Yan J and Li B: The clinical outcome, pathologic spectrum, and genomic landscape for 454 cases of salivary mucoepidermoid carcinoma. NPJ Precis Oncol 8: 238, 2024.
5. Ullah A, Khan J, Waheed A, Karki NR, Goodbee M, Yasinzai AQK, Tareen B, Wali A, Khan KA, Zarak MS, *et al*: Mucoepidermoid carcinoma of the salivary gland: Demographics and comparative analysis in U.S. children and adults with future perspective of management. Cancers (Basel) 15: 250, 2022.
6. Zhou Z, Mai Y, Zhang G, Wang Y, Sun P, Jing Z, Li Z, Xu Y, Han B and Liu J: Emerging role of immunogenic cell death in cancer immunotherapy: Advancing next generation CAR-T cell immunotherapy by combination. Cancer Lett 598: 217079, 2024.
7. Babiker R, Wali AF, El-Tanani M, Rabbani SA, Rangraze I, Satyam SM, Patni MA and El-Tanani Y: Comparative efficacy of immune checkpoint inhibitors and therapeutic vaccines in solid tumors: A systematic review and meta-analysis of randomized controlled trials. Vaccines 13: 423, 2025.
8. Galluzzi L, Vitale I, Warren S, Adjemian S, Agostinis P, Martinez AB, Chan TA, Coukos G, Demaria S, Deutsch E, *et al*: Consensus guidelines for the definition, detection and interpretation of immunogenic cell death. J Immunother Cancer 8: e000337, 2020.
9. Alzeibak R, Mishchenko TA, Shilyagina NY, Balalaeva IV, Vedunova MV and Krysko DV: Targeting immunogenic cancer cell death by photodynamic therapy: Past, present and future. J Immunother Cancer 9: e001926, 2021.
10. Lin Y, Lin P, Xu R, Chen X, Lu Y, Zheng J, Zheng Y, Zhou Z, Mai Z, Zhao X and Cui L: Nanovaccines empowering $CD8^+$T cells: A precision strategy to enhance cancer immunotherapy. Theranostics 15: 3098-3121, 2025.
11. Jurišić V, Bogdanović G, Kojic V, Jakimov D and Srdic T: Effect of TNF-alpha on Raji cells at different cellular levels estimated by various methods. Ann Hematol 85: 86-94, 2006.
12. Jurišić V, Bogdanović G, Srdić T, Jakimov D, Mrdjanović J, Baltić M and Baltić VV: Modulation of TNF-α activity in tumor PC cells using anti-CD45 and anti-CD95 monoclonal antibodies. Cancer Lett 214: 55-61, 2004.
13. Jan CI, Tsai MH, Chiu CF, Huang YP, Liu CJ and Chang NW: Fenofibrate suppresses oral tumorigenesis via reprogramming metabolic processes: Potential drug repurposing for oral cancer. Int J Biol Sci 12: 786-798, 2016.
14. Bolhassani A and Agi E: Heat shock proteins in infection. Clin Chim Acta 498: 90-100, 2019.
15. Lamberti MJ, Mentucci FM, Roselli E, Araya P, Rivarola VA, Vittar NB and Maccioni M: Photodynamic modulation of type 1 interferon pathway on melanoma cells promotes dendritic cell activation. Front Immunol 10: 2614, 2019.
16. Bianchi ME, Crippa MP, Manfredi AA, Mezzapelle R, Querini PR and Venereau E: High-mobility group box 1 protein orchestrates responses to tissue damage via inflammation, innate and adaptive immunity, and tissue repair. Immunol Rev 280: 74-82, 2017.
17. Yadollahvandmiandoab R, Jalalizadeh M, Buosi K, Garcia-Perdomo HA and Reis LO: Immunogenic cell death role in urothelial cancer therapy. Curr Oncol 29:6700-6713, 2022.
18. Niu X, Chen L, Li Y, Hu Z and He F: Ferroptosis, necroptosis, and pyroptosis in the tumor microenvironment: Perspectives for immunotherapy of SCLC. Semin Cancer Biol 86: 273-285, 2022.
19. Wang X, Liu X, Chen Y, Wang H, Zhang R, Zhang Q, Wei Y, Shi S and Li X: Calreticulin regulated intrinsic apoptosis through mitochondria-dependent and independent pathways mediated by ER stress in arsenite exposed HT-22 cells. Chemosphere 251: 126466, 2020.
20. Feng K, Ge Y, Chen Z, Li X, Liu Z, Li X, Li H, Tang T, Yang F and Wang X: Curcumin inhibits the PERK-eIF2α-CHOP pathway through promoting SIRT1 expression in oxidative stress-induced rat chondrocytes and ameliorates osteoarthritis progression in a rat model. Oxid Med Cell Longev 2019: 8574386, 2019.

21. Yang P, Jiang PW, Li C, Gao MX, Sun YS, Zhang DY, Du WQ, Zhao J, Shi ST, Li Y, *et al*: Cdc25C/cdc2/cyclin B, raf/MEK/ERK and PERK/eIF2α/CHOP pathways are involved in forskolin-induced growth inhibition of MM.1S cells by G2/M arrest and mitochondrion-dependent apoptosis. Cell Cycle 20: 2402-2412, 2021.
22. Liu Y, Sun L, Ma Y, Wei B, Gao M and Shang L: High glucose and bupivacaine-induced cytotoxicity is mediated by enhanced apoptosis and impaired autophagy via the PERK-ATF4-CHOP and IRE1-TRAF2 signaling pathways. Mol Med Rep 20:2832-2842, 2019.
23. Jiang M, Zeng J, Zhao L, Zhang M, Ma J, Guan X and Zhang W: Chemotherapeutic drug-induced immunogenic cell death for nanomedicine-based cancer chemo-immunotherapy. Nanoscale 13: 17218-17235, 2021.
24. Li Y, Liu X, Zhang X, Pan W, Li N and Tang B: Immunogenic cell death inducers for enhanced cancer immunotherapy. Chem Commun (Camb) 57: 12087-12097, 2021.
25. Li Z, Lai X, Fu S, Ren L, Cai H, Zhang H, Gu Z, Ma X and Luo K: Immunogenic cell death activates the tumor immune microenvironment to boost the immunotherapy efficiency. Adv Sci (Weinh) 9: e2201734, 2022.
26. Fu L, Ma X, Liu Y, Xu Z and Sun Z: Applying nanotechnology to boost cancer immunotherapy by promoting immunogenic cell death. Chin Chem Lett 33: 1718-1728, 2022.
27. Veld RV, Heuts J, Ma S, Cruz LJ, Ossendorp FA and Jager MJ: Current challenges and opportunities of photodynamic therapy against cancer. Pharmaceutics 15: 330, 2023.
28. Ramchandani D and Mittal V: Thrombospondin in tumor microenvironment. Adv Exp Med Biol 1272: 133-147, 2020.
29. Miao WM, Seng WL, Duquette M, Lawler P, Laus C and Lawler J: Thrombospondin-1 type 1 repeat recombinant proteins inhibit tumor growth through transforming growth factor-beta-dependent and -independent mechanisms. Cancer Res 61: 7830-7839, 2001.
30. Uscanga-Palomeque AC, Calvillo-Rodríguez KM, Gómez-Morales L, Lardé E, Denèfle T, Caballero-Hernández D, Merle-Béral H, Susin SA, Karoyan P, Martínez-Torres AC and Rodríguez-Padilla C: CD47 agonist peptide PKHB1 induces immunogenic cell death in T-cell acute lymphoblastic leukemia cells. Cancer Sci 110: 256-268, 2019.
31. Zhu Y, Cai K, Guo L, Zhang H, Guan L, Zhang Z, Huang P and Yang S: Thrombospondin-1 induces immunogenic cell death in human mucoepidermoid carcinoma MC-3 cells via the PERK/eIF2α signaling pathway: Potential implications for tumor immunotherapy. Discov Oncol 16: 576, 2025.
32. Chomczynski P and Sacchi N: The single-step method of RNA isolation by acid guanidinium thiocyanate-phenol-chloroform extraction: Twenty-something years on. Nat Protoc 1: 581-585, 2006.
33. Livak KJ and Schmittgen TD: Analysis of relative gene expression data using real-time quantitative PCR and the 2(-Delta Delta C(T)) method. Methods 25: 402-408, 2001.
34. Obradović J, Todosijević J and Jurišić V: Application of the conventional and novel methods in testing EGFR variants for NSCLC patients in the last 10 years through different regions: A systematic review. Mol Biol Rep 48: 3593-3604, 2021.
35. Jurisic V, Srdic-Rajic T, Konjevic G, Bogdanovic G and Colic M: TNF-α induced apoptosis is accompanied with rapid CD30 and slower CD45 shedding from K-562 cells. J Membr Biol 239: 115-122, 2011.
36. Li Y, Guo Y, Tang J, Jiang J and Chen Z: New insights into the roles of CHOP-induced apoptosis in ER stress. Acta Biochim Biophys Sin (Shanghai) 46: 629-640, 2014.
37. Garg AD, More S, Rufo N, Mece O, Sassano ML, Agostinis P, Zitvogel L, Kroemer G and Galluzzi L: Trial watch: Immunogenic cell death induction by anticancer chemotherapeutics. Oncoimmunology 6: e1386829, 2017.
38. Jurišić V, Bumbaširević V, Konjević G, Djuričič B and Spužić I: TNF-alpha induces changes in LDH isotype profile following triggering of apoptosis in PBL of non-Hodgkin's lymphomas. Ann Hematol 83: 84-91, 2004.
39. Atkin-Smith GK: Phagocytic clearance of apoptotic, necrotic, necroptotic and pyroptotic cells. Biochem Soc Trans 49: 793-804, 2021.
40. Meng Q, Ding B, Ma P and Lin J: Interrelation between programmed cell death and immunogenic cell death: Take antitumor nanodrug as an example. Small Methods 7: e2201406, 2023.
41. Menger L, Vacchelli E, Adjemian S, Martins I, Ma Y, Shen S, Yamazaki T, Sukkurwala AQ, Michaud M, Mignot G, *et al*: Cardiac glycosides exert anticancer effects by inducing immunogenic cell death. Sci Transl Med 4: 143ra99, 2012.
42. Kepp O, Menger L, Vacchelli E, Locher C, Adjemian S, Yamazaki T, Martins I, Sukkurwala AQ, Michaud M, Senovilla L, *et al*: Crosstalk between ER stress and immunogenic cell death. Cytokine Growth Factor Rev 24: 311-318, 2013.
43. Chen C, Chen H, Zhang Y, Thomas HR, Frank MH, He Y and Xia R: TBtools: An integrative toolkit developed for interactive analyses of big biological data. Mol Plant 13: 1194-1202, 2020.
44. Kim DY, Pyo A, Yun M, Thangam R, You SH, Zhang Y, Jung YR, Nguyen DH, Venu A, Kim HS, *et al*: Imaging calreticulin for early detection of immunogenic cell death during anticancer treatment. J Nucl Med 62: 956-960, 2021.
45. Turubanova VD, Balalaeva IV, Mishchenko TA, Catanzaro E, Alzeibak R, Peskova NN, Efimova I, Bachert C, Mitroshina EV, Krysko O, *et al*: Immunogenic cell death induced by a new photodynamic therapy based on photosens and photodithazine. J Immunother Cancer 7: 350, 2019.
46. Ni K, Luo T, Nash GT and Lin W: Nanoscale metal-organic frameworks for cancer immunotherapy. Acc Chem Res 53: 1739-1748, 2020.
47. Turubanova VD, Mishchenko TA, Balalaeva IV, Efimova I, Peskova NN, Klapshina LG, Lermontova SA, Bachert C, Krysko O, Vedunova MV and Krysko DV: Novel porphyrazine-based photodynamic anti-cancer therapy induces immunogenic cell death. Sci Rep 11: 7205, 2021.
48. Li X, Zheng J, Chen S, Meng FD, Ning J and Sun SL: Oleandrin, a cardiac glycoside, induces immunogenic cell death via the PERK/elF2α/ATF4/CHOP pathway in breast cancer. Cell Death Dis 12: 314, 2021.
49. Wang M, Zhao L, Tong D, Yang L, Zhu H, Li Q and Zhang F: BET bromodomain inhibitor JQ1 promotes immunogenic cell death in tongue squamous cell carcinoma. Int Immunopharmacol 76: 105921, 2019.
50. Sevilla-Montero J, Bienes-Martínez R, Labrousse-Arias D, Fuertes-Yebra E, Ordóñez Á and Calzada MJ: pVHL-mediated regulation of the anti-angiogenic protein thrombospondin-1 decreases migration of clear cell renal carcinoma cell lines. Sci Rep 10: 1175, 2020.
51. Fu X, Cui J, Meng X, Jiang P, Zheng Q, Zhao W and Chen X: Endoplasmic reticulum stress, cell death and tumor: Association between endoplasmic reticulum stress and the apoptosis pathway in tumors (Review). Oncol Rep 45: 801-808, 2021.

Copyright © 2026 Bao et al. This work is licensed under a Creative Commons Attribution-NonCommercial-NoDerivatives 4.0 International (CC BY-NC-ND 4.0) License.